Non-parametric Identification of Viscoelastic Materials from Wave Propagation Experiments*

M. Mossberg[†], L. Hillström[‡] and T. Söderström[†]

January 12, 2000

Abstract

We investigate how the frequency-dependent wave propagation coefficient and complex modulus for a linearly viscoelastic material can be estimated from wave propagation experiments. The strains at different sections of a bar specimen are measured as functions of time. The time series are transformed into the frequency domain, where a non-parametric identification is made. A thorough analysis of the quality of the non-parametric estimate is made, in which approximate expressions for the covariance matrices of the wave propagation coefficient and the complex modulus are derived. The validity of these expressions are confirmed by numerical studies and real experiments.

Keywords: Identification, material functions, complex modulus, linear viscoelastic, wave propagation, accuracy.

1 Introduction

The frequency-dependent complex modulus relates stress and strain of a linearly viscoelastic material. Polymers are examples of materials that can be approximated as linearly viscoelastic. In order to make efficient use of engineering materials with viscoelastic behaviour, it is important to know their complex moduli at relevant frequencies and temperatures. If such materials are to be used in components and structures which are loaded dynamically, e.g., through impact, then frequencies of interest may commonly vary from 100 Hz to 10 kHz. In this frequency range, wave propagation methods are well suited for the determination of complex modulus.

An experiment as in Figure 1 is carried out. A bar specimen is axially impacted, and as a result waves start to propagate through the bar. The waves are associated with strains in the material, and from known strains $\varepsilon_1, \varepsilon_2, \dots, \varepsilon_n$ at $n \geq 3$ different sections located at $x_1, x_2, \dots, x_n$ one can determine the complex modulus. These strains may be known either from measurements or from a free-end boundary condition. It turns out that it is difficult to obtain estimates of good quality at certain frequencies. One set of critical frequencies corresponds to conditions such that the distances between the sections considered become integral multiples of a half wavelength. It is therefore important to know how the sensors

*Work supported by Swedish Research Council for Engineering Sciences under contracts 96–212 and 98–137.

[†]Dept. of Systems and Control, Information Technology, Uppsala University, P.O. Box 27, SE-751 03 Uppsala, Sweden, E-mail: {mm,ts}@syscon.uu.se

[‡]Ångström Laboratory, Uppsala University, P.O. Box 534, SE-751 21 Uppsala, Sweden, E-mail: lars.hillstrom@material.uu.se

should be placed in order to extract as much information as possible from the known strains.

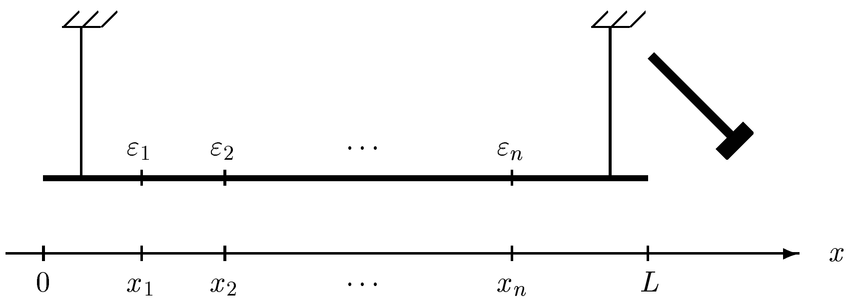

Figure 1: Experiment. When the hammer hits the right end of the bar specimen, waves are generated. The complex modulus can be determined from the strains $\varepsilon_1, \varepsilon_2, \dots, \varepsilon_n$ known from measurements and from a free-end boundary condition.

This problem, and closely related ones, have been studied in several earlier papers, see for example [1,2,4–7,10]. An analysis of the quality of the estimate is absent in most papers. An exception is [2] where the effect of errors, both measurement and numerical, are discussed. The main purpose of this paper is therefore to provide an analysis of how the estimated complex modulus is affected by stochastic disturbances, such as measurement noise, of the measured strains.

A model for the wave propagation in the bar specimen is given in the next section. A non-parametric identification method of the material functions is described in Section 3. The analysis of the accuracy of the estimated material functions is made in Section 4. Numerical studies are carried out in Section 5, while results from real experiments are treated in Section 6. Finally, conclusions are drawn in Section 7. Throughout the paper, vectors are denoted with bold-face lower case letters and matrices are denoted with bold-face capital letters.

2 Model

The wave propagation in the bar is described by

$$c^2 * \frac{\partial^2 \varepsilon(x,t)}{\partial x^2} = \frac{\partial^2 \varepsilon(x,t)}{\partial t^2}, \tag{1}$$

$$c^2 = \mathcal{F}^{-1}\Big\{\frac{E(\omega)}{\rho}\Big\}, \tag{2}$$

see Appendix A, where $\varepsilon(x,t)$ is the axial strain at section x and time t, ω is the angular frequency, $E(\omega)$ is the complex modulus, ρ is the density, $*$ is the convolution operator and $\mathcal{F}^{-1}$ denotes inverse Fourier transformation. The corresponding description in the frequency domain is given by

$$\frac{E(\omega)}{\rho}\frac{\partial^2 \hat{\varepsilon}(x,\omega)}{\partial x^2} = -\omega^2 \hat{\varepsilon}(x,\omega), \tag{3}$$

where $\hat{\varepsilon}(x,\omega)$ is the Fourier transform of $\varepsilon(x,t)$. Equation (3) can also be written as

$$\frac{\partial^2 \hat{\varepsilon}(x,\omega)}{\partial x^2} - \gamma^2(\omega)\hat{\varepsilon}(x,\omega) = 0, \tag{4}$$

where the wave propagation coefficient $\gamma(\omega)$ and the complex modulus $E(\omega)$ are related through

$$\gamma^2(\omega) = -\frac{\rho\omega^2}{E(\omega)}. \tag{5}$$

For linearly elastic materials, such as steel, $E(\omega)$ is real valued and constant (the modulus of elasticity or Young's modulus), $\gamma(\omega)$ is imaginary valued, c is real valued and constant (the phase velocity of the waves), and (1) is the ordinary wave equation.

The general solution of (4) is

$$\hat{\varepsilon}(x,\omega) = \hat{P}(\omega)e^{-\gamma(\omega)x} + \hat{N}(\omega)e^{\gamma(\omega)x}, \tag{6}$$

where $\hat{P}(\omega)$ and $\hat{N}(\omega)$ are complex valued functions of ω which can be interpreted as amplitudes of waves at $x = 0$ going rightwards and leftwards, respectively. The boundary conditions

$$\hat{\varepsilon}(0,\omega) = 0, \tag{7}$$

$$\hat{\varepsilon}(L,\omega) = \hat{\Phi}(\omega) \tag{8}$$

are assumed, where $\hat{\Phi}(\omega)$ denotes the Fourier transform of the strain pulse generated at the right end of the bar specimen. The boundary condition (7) represents the free left end.

3 A non-parametric identification technique

Strains $\varepsilon(x_j,t_k)$ are assumed to be at sections x_j, with $j = 1,\ldots,n$, at times t_k, with $k = 1,\ldots,N$, where N is the number of samples. After Fourier transformation we get $\hat{\varepsilon}_j(\omega_k) = \hat{\varepsilon}(x_j,\omega_k)$ for frequencies

$$\omega_k = \frac{2\pi k}{N\Delta t}, \qquad k = 1,\ldots,N, \tag{9}$$

where Δt is the sampling interval. From these data, the wave propagation coefficient $\gamma(\omega_k)$ and the complex modulus $E(\omega_k)$ are to be determined for every frequency ω_k.

In this section, we will describe a *non-parametric* method for identifying the wave propagation coefficient $\gamma(\omega_k)$. When this has been done, the complex modulus $E(\omega_k)$ can be obtained from (5). By using (6), we can form the nonlinear and overdetermined system of equations

$$\mathbf{A}\big(\gamma(\omega_k)\big)\begin{bmatrix}\hat{P}(\omega_k)\\ \hat{N}(\omega_k)\end{bmatrix} = \hat{\boldsymbol{\varepsilon}}(\omega_k), \tag{10}$$

where

$$\mathbf{A}\big(\gamma(\omega_k)\big) = \begin{bmatrix} e^{-\gamma(\omega_k)x_1} & e^{\gamma(\omega_k)x_1}\\ \vdots & \vdots\\ e^{-\gamma(\omega_k)x_n} & e^{\gamma(\omega_k)x_n}\end{bmatrix}, \tag{11}$$

$$\hat{\boldsymbol{\varepsilon}}(\omega_k) = \begin{bmatrix}\hat{\varepsilon}_1(\omega_k) & \cdots & \hat{\varepsilon}_n(\omega_k)\end{bmatrix}^T, \tag{12}$$

for the unknowns $\gamma(\omega_k)$, $\hat{P}(\omega_k)$ and $\hat{N}(\omega_k)$. In order to estimate $\gamma(\omega_k)$, we introduce the loss function

$$U\big(\gamma(\omega_k),\hat{P}(\omega_k),\hat{N}(\omega_k)\big) = \left\|\hat{\boldsymbol{\varepsilon}}(\omega_k) - \mathbf{A}\big(\gamma(\omega_k)\big)\begin{bmatrix}\hat{P}(\omega_k)\\ \hat{N}(\omega_k)\end{bmatrix}\right\|^2, \tag{13}$$

which we wish to minimise with respect to $\gamma(\omega_k)$, $\hat{P}(\omega_k)$ and $\hat{N}(\omega_k)$. Since this is a separable least squares problem, we minimise (13) with respect to $\hat{P}(\omega_k)$ and $\hat{N}(\omega_k)$ for a given $\gamma(\omega_k)$, i.e.,

$$\begin{bmatrix} \hat{P}_{\text{est}}(\omega_k) \\ \hat{N}_{\text{est}}(\omega_k) \end{bmatrix} = \arg \min_{\hat{P}(\omega_k), \hat{N}(\omega_k)} U\big(\gamma(\omega_k), \hat{P}(\omega_k), \hat{N}(\omega_k)\big). \tag{14}$$

The solution of (14) is given by

$$\begin{bmatrix} \hat{P}_{\text{est}}(\omega_k) \\ \hat{N}_{\text{est}}(\omega_k) \end{bmatrix} = \mathbf{A}^{\dagger}\big(\gamma(\omega_k)\big)\hat{\boldsymbol{\varepsilon}}(\omega_k), \tag{15}$$

where $\mathbf{A}^{\dagger} = (\mathbf{A}^{*}\mathbf{A})^{-1}\mathbf{A}^{*}$ is the pseudoinverse of $\mathbf{A}$.Now, consider the concentrated loss function

$$W\big(\gamma(\omega_k)\big) \triangleq U\big(\gamma(\omega_k), \hat{P}_{\text{est}}(\omega_k), \hat{N}_{\text{est}}(\omega_k)\big) = \Big\|\hat{\boldsymbol{\varepsilon}}(\omega_k) - \mathbf{A}\big(\gamma(\omega_k)\big)\mathbf{A}^{\dagger}\big(\gamma(\omega_k)\big)\hat{\boldsymbol{\varepsilon}}(\omega_k)\Big\|^2 \tag{16}$$

from which an estimate of the complex valued $\gamma_{\text{est}}(\omega_k)$ is obtained as

$$\gamma_{\text{est}}(\omega_k) = \arg \min_{\gamma(\omega_k)} W\big(\gamma(\omega_k)\big). \tag{17}$$

The solution of (17) is discussed in Section 6.2.

Remark When $n = 3$, the system of equations (10) has, in the case of equidistantly spaced sensors, one exact solution for $\hat{P}(\omega_k)$, $\hat{N}(\omega_k)$ and $\gamma(\omega_k)$. See [4] for an analysis of this case.

4 Analysis of accuracy

We will first derive an asymptotic expression for the accuracy of the estimated wave propagation coefficient (17), which is valid when the signal-to-noise ratio (SNR) tends to infinity. Secondly, we will establish the corresponding expression for the complex modulus. To be more specific, a vector $\boldsymbol{\varepsilon}(t_k)$ of measured strains at time t_k is assumed to equal a vector $\boldsymbol{\epsilon}(t_k)$ of *true* and *unknown* strains plus a stochastic disturbance $\mathbf{v}(t_k)$,

$$\boldsymbol{\varepsilon}(t_k) = \boldsymbol{\epsilon}(t_k) + \mathbf{v}(t_k). \tag{18}$$

Our analysis covers the case when the noise $\mathbf{v}(t_k)$ is small in comparison to $\boldsymbol{\epsilon}(t_k)$, but non-negligible.

For the loss function $W\big(\gamma(\omega_k)\big)$ given by (16) it holds that $W\big(\gamma(\omega_k)\big) : \mathbb{C} \to \mathbb{R}$. If we instead consider $W\big(\gamma(\omega_k)\big) = V\big(\mathbf{g}(\omega_k)\big)$, where the elements of the vector

$$\mathbf{g}(\omega_k) = \begin{bmatrix} \gamma_r(\omega_k) & \gamma_i(\omega_k) \end{bmatrix}^T \tag{19}$$

are the real- and imaginary parts of $\gamma(\omega_k)$, it holds that $V\big(\mathbf{g}(\omega_k)\big) : \mathbb{R}^2 \to \mathbb{R}$. This means that we can use only real valued variables in the analysis. The real part $\gamma_r(\omega_k)$ can be interpreted as the damping coefficient and the imaginary part $\gamma_i(\omega_k)$ as the wavenumber. They are usually denoted $\alpha(\omega_k)$ and $k(\omega_k)$, respectively.

Since $\mathbf{g}_{\text{est}}(\omega_k)$ minimises $V\big(\mathbf{g}(\omega_k)\big)$ and thereby (16), we have that

$$\mathbf{V}'\big(\mathbf{g}_{\text{est}}(\omega_k)\big) = \mathbf{0}, \tag{20}$$

where $\mathbf{V}'\big(\mathbf{g}(\omega_k)\big)$ is the gradient vector of $V\big(\mathbf{g}(\omega_k)\big)$. Assume that the estimated wave propagation coefficient converges to

$$\mathbf{g}_{\infty}(\omega_k) = \lim_{\text{SNR}\to\infty} \mathbf{g}_{\text{est}}(\omega_k), \tag{21}$$

as the SNR tends to infinity, which corresponds to noise-free measurements of the strains. Next, we make a Taylor series expansion around $\mathbf{g}_{\infty}(\omega_k)$ under the assumption that the SNR is large and obtain

$$\mathbf{0} = \mathbf{V}'\big(\mathbf{g}_{\text{est}}(\omega_{\mathbf{k}})\big) = \mathbf{V}'\big(\mathbf{g}_{\infty}(\omega_{\mathbf{k}})\big) + \mathbf{V}''\big(\mathbf{g}_{\infty}(\omega_{\mathbf{k}})\big)\big(\mathbf{g}_{\text{est}}(\omega_{\mathbf{k}}) - \mathbf{g}_{\infty}(\omega_{\mathbf{k}})\big) + \dots, \tag{22}$$

where $\mathbf{V}''\big(\mathbf{g}(\omega_k)\big)$ is the Hessian matrix of $V\big(\mathbf{g}(\omega_k)\big)$. This gives

$$\tilde{\mathbf{g}}(\omega_k) \triangleq \mathbf{g}_{\text{est}}(\omega_k) - \mathbf{g}_{\infty}(\omega_k) \approx -\big[\mathbf{V}''\big(\mathbf{g}_{\infty}(\omega_k)\big)\big]^{-1}\mathbf{V}'\big(\mathbf{g}_{\infty}(\omega_k)\big). \tag{23}$$

We also assume that

$$\lim_{\text{SNR}\to\infty} \mathbf{V}''\big(\mathbf{g}_{\infty}(\omega_k)\big) = \mathbf{H}(\omega_k), \tag{24}$$

where $\mathbf{H}(\omega_k) > \mathbf{0}$ is a positive definite matrix. The following result can now be given:

Result 1 *The correlation between the estimation errors of the wave propagation coefficient at frequencies ω_a and ω_b can be described through*

$$\mathrm{E}\{\tilde{\mathbf{g}}(\omega_a)\tilde{\mathbf{g}}^T(\omega_b)\} \approx \mathbf{H}^{-1}(\omega_a)\mathbf{G}(\omega_a,\omega_b)\mathbf{H}^{-T}(\omega_b), \tag{25}$$

where

$$\mathbf{G}(\omega_a,\omega_b) = \mathrm{E}\Big\{\mathbf{V}'\big(\mathbf{g}_{\infty}(\omega_a)\big)\big[\mathbf{V}'\big(\mathbf{g}_{\infty}(\omega_b)\big)\big]^T\Big\}. \tag{26}$$

□

To calculate the matrix (25), we need expressions for $\mathbf{H}(\omega_k)$ and $\mathbf{G}(\omega_a,\omega_b)$. In Appendix B it is shown that $\mathbf{H}(\omega_k)$ can be expressed as

$$\mathbf{H}(\omega_k) = \begin{bmatrix} \hat{\boldsymbol{\epsilon}}^*(\omega_k)\mathbf{B}_{rr}(\omega_k)\hat{\boldsymbol{\epsilon}}(\omega_k) & \hat{\boldsymbol{\epsilon}}^*(\omega_k)\mathbf{B}_{ri}(\omega_k)\hat{\boldsymbol{\epsilon}}(\omega_k) \\ \hat{\boldsymbol{\epsilon}}^*(\omega_k)\mathbf{B}_{ir}(\omega_k)\hat{\boldsymbol{\epsilon}}(\omega_k) & \hat{\boldsymbol{\epsilon}}^*(\omega_k)\mathbf{B}_{ii}(\omega_k)\hat{\boldsymbol{\epsilon}}(\omega_k) \end{bmatrix} \tag{27}$$

where $\mathbf{B}_{rr}(\omega_k)$, $\mathbf{B}_{ri}(\omega_k)$, $\mathbf{B}_{ir}(\omega_k)$ and $\mathbf{B}_{ii}(\omega_k)$ are defined in (65)–(68), while $\mathbf{G}(\omega_a,\omega_b)$ is given in Lemma 1.

Lemma 1 *Assume $\mathbf{v}(t_k)$ in (18) to be spatially and temporally white Gaussian noise, i.e.*

$$\mathbf{v}(t_k) \sim \mathcal{N}(\mathbf{0},\sigma^2\mathbf{I}), \qquad \forall\, t_k \tag{28}$$

$$\mathrm{E}\mathbf{v}(t_a)\mathbf{v}^T(t_b) = \delta_{a,b}\sigma^2\mathbf{I}, \tag{29}$$

where $\delta_{a,b}$ is the Kronecker delta. Under this assumption, the elements of $\mathbf{G}(\omega_a,\omega_b)$, defined in (26), are given by

$$\mathbf{G}_{11}(\omega_a,\omega_b) = \begin{cases} 0 & \text{if } a \neq b, \\ \sigma^4 N^2 \mathrm{tr}\big\{\mathbf{P}_r^2(\omega_a)\big\} + 2\sigma^2 N \hat{\boldsymbol{\epsilon}}^*(\omega_a)\mathbf{P}_r^2(\omega_a)\hat{\boldsymbol{\epsilon}}(\omega_a) & \text{if } a = b \end{cases} \tag{30}$$

and

$$\mathbf{G}_{12}(\omega_a,\omega_b) = 0, \qquad \forall\, a,b, \tag{31}$$

where tr *denotes the trace operator and where $\mathbf{P}_r(\omega_k)$ is defined in (61). The element $\mathbf{G}_{21}(\omega_a,\omega_b) = \mathbf{G}_{12}(\omega_a,\omega_b)$, and the element $\mathbf{G}_{22}(\omega_a,\omega_b)$ is obtained by changing $\mathbf{P}_r(\omega_k)$ to $\mathbf{P}_i(\omega_k)$ in (30), where $\mathbf{P}_i(\omega_k)$ is defined in (62).*

□

Proof See Appendix C. $\square$

Remark If the noise $\mathbf{v}(t_k)$ is not Gaussian, (30) and (31) will be slightly modified. More precisely, (86) in Appendix C will be different since the first and third order moments are not necessarily zero for non–Gaussian variables. A larger source of error might be that we have not considered the fact that one section may be free from measurement noise. It is the free end where the strains are known to be zero and are therefore not measured. The results in Sections 5 and 6 do not, however, indicate that this affects the reliability of the accuracy expression (25) in Result 1. $\square$

When the wave propagation coefficient $\gamma(\omega_k)$ is known, the complex modulus $E(\omega_k)$ can be obtained from (5) as

$$E(\omega_k) = -\frac{\rho\omega_k^2}{\gamma^2(\omega_k)}. \tag{32}$$

Let

$$\mathbf{e}(\omega_k) = \begin{bmatrix} E_r(\omega_k) & E_i(\omega_k) \end{bmatrix}^T, \tag{33}$$

where $E_r(\omega_k)$ and $E_i(\omega_k)$ denote the real and imaginary parts of $E(\omega_k)$, respectively. Write (32) as

$$\mathbf{e}(\omega_k) = \mathbf{f}\big(\mathbf{g}(\omega_k)\big) = \begin{bmatrix} f_1\big(\mathbf{g}(\omega_k)\big) & f_2\big(\mathbf{g}(\omega_k)\big) \end{bmatrix}^T, \tag{34}$$

where $\mathbf{f}\big(\mathbf{g}(\omega_k)\big) : \mathbb{R}^2 \to \mathbb{R}^2$ and

$$f_1\big(\mathbf{g}(\omega_k)\big) = \frac{-\rho\omega_k^2\big(\gamma_r^2(\omega_k) - \gamma_i^2(\omega_k)\big)}{\big(\gamma_r^2(\omega_k) + \gamma_i^2(\omega_k)\big)^2}, \tag{35}$$

$$f_2\big(\mathbf{g}(\omega_k)\big) = \frac{2\rho\omega_k^2\gamma_r(\omega_k)\gamma_i(\omega_k)}{\big(\gamma_r^2(\omega_k) + \gamma_i^2(\omega_k)\big)^2}. \tag{36}$$

Result 2 *The correlation between the estimation errors of the complex modulus at frequencies ω_a and ω_b can be described through*

$$\mathrm{E}\{\tilde{\mathbf{e}}(\omega_a)\tilde{\mathbf{e}}^T(\omega_b)\} \approx \frac{\partial \mathbf{f}\big(\mathbf{g}(\omega_a)\big)}{\partial \mathbf{g}(\omega_a)} \mathrm{E}\{\tilde{\mathbf{g}}(\omega_a)\tilde{\mathbf{g}}^T(\omega_b)\} \left[\frac{\partial \mathbf{f}\big(\mathbf{g}(\omega_b)\big)}{\partial \mathbf{g}(\omega_b)}\right]^T, \tag{37}$$

where

$$\frac{\partial \mathbf{f}\big(\mathbf{g}(\omega_k)\big)}{\partial \mathbf{g}(\omega_k)} = \begin{bmatrix} \dfrac{\partial f_1\big(\mathbf{g}(\omega_k)\big)}{\partial \gamma_r(\omega_k)} & \dfrac{\partial f_1\big(\mathbf{g}(\omega_k)\big)}{\partial \gamma_i(\omega_k)} \\ \dfrac{\partial f_2\big(\mathbf{g}(\omega_k)\big)}{\partial \gamma_r(\omega_k)} & \dfrac{\partial f_2\big(\mathbf{g}(\omega_k)\big)}{\partial \gamma_i(\omega_k)} \end{bmatrix}. \tag{38}$$

$\square$

5 Numerical example

5.1 Data from numerical simulations

The experiment described in Section 1 and the non-parametric identification in Section 3 were considered in a Monte Carlo simulation in order to investigate the validity of expression (25) of Result 1. Data for the wave propagation coefficient were generated from the standard linear solid model, see Appendix D. The Fourier transformed strains were then obtained from (6).

Since the measurements of the strains are made in the time domain and are affected by noise as in (18), the Fourier transformed strains were inversely transformed to the time domain where noise was added. The procedure of adding noise to the time domain data, transforming the data to the frequency domain and making an estimation was repeated 100 times for different noise realisations with variance $\sigma^2 = 1 \cdot 10^{-18}$. The maximum absolute value of the true strain $\epsilon_j(t_k)$ was of the order 6 μm/m. The length of the bar was $L = 2$ m, the number of data $N = 20\,001$ and the sampling interval $\Delta t = 10$ μs. The strain pulse $\hat{\Phi}(\omega)$ at the right end of the bar was chosen so that a sufficient excitation for all considered frequencies was obtained, see Section 5.2. Moreover, the parameters in the standard linear solid model were $E_1 = 56$ GPa, $E_2 = 5.6$ GPa and $\eta = 2$ MPa·s. With this choice of the viscoelastic parameters, the standard linear solid model applies to the dynamic behavior of PMMA (plexiglass), a material with density $\rho = 1180$ kg/m^3. The locations of the sections were $x = \{0, 0.290, 0.646, 1.078, 1.600\}$ m, i.e., the free end was used where we know that the strains are zero. However, noise was added also to the free end strains.

The standard deviations of the estimates from the 100 simulated experiments were then compared to the ones given by the square roots of the diagonal elements in (25). Note that $\mathbf{g}_\infty(\omega_k)$ in (25) was calculated from the standard linear solid model with (116) and (5). The result of such a comparison is shown in Figure 2.

5.2 Discussion

The two results are in accordance. Hence, the validity of (25) is confirmed by the numerical studies. The standard deviations given by (25) can be computed from a *single* realisation. In this way the estimated wave propagation coefficient $\gamma(\omega_k) = \gamma_r(\omega_k) + \mathrm{i}\gamma_i(\omega_k)$, where $\gamma_r(\omega_k) \equiv \alpha(\omega_k)$ and $\gamma_i(\omega_k) \equiv k(\omega_k)$, can be given a 'quality tag' that expresses the confidence in the estimate.

The positions of the sensors greatly affect the quality of the estimated results and may lead to very poor accuracy in some frequency regions. Particularly, the case with equidistantly spaced sensors should be avoided. Suitable positions of the sensors make it possible to get much information out of the measurements. A discussion of problems associated with certain sensor configurations together with a motivation why the locations used in the simulations are a suitable choice can be found in [4].

It can be noted that the standard deviations "oscillate" with the frequency in Figure 2. The oscillations can be interpreted as a consequence of the bar's eigenmodes. We have found that the valleys of the curves coincide with the eigenfrequencies of the bar. The reason for this is that the SNR is high at those frequencies. The regular oscillations are due to the fact that the eigenfrequencies are more or less uniformly distributed along the frequency axis. The eigenfrequencies are obtained from the solution of (4) with the boundary conditions

$$\hat{\varepsilon}(0, \omega) = \hat{\varepsilon}(L, \omega) = 0. \tag{39}$$

After some calculations, the real part of the eigenfrequency for eigenmode m is approximately given as

$$\omega_m = \pm \frac{m\pi}{L} \sqrt{\frac{E_r(\omega_m)}{\rho}}, \qquad m = 1, 2, \ldots . \tag{40}$$

In the case of the standard linear solid, the real part of the complex modulus, E_r, is approximately constant. It can be noted that the neglected imaginary part of the eigenfrequency is a measure of the damping of the eigenmode.

In the analysis it is assumed that measurements from all sections are corrupted by noise. In practice, however, the free end is used where it is known that the strains are exactly zero. Therefore, one of the strain data series is noise free. This can be taken into account by lowering the variance σ^2 of the noise, used in the analytic expression for the expected accuracy. To find out how much, a Monte Carlo simulation similar to that in Section 5.1 was carried out. Measurement noise with the same variance as in the simulation described in Section 5.1 was added to all strain data series except for the one corresponding to the free end. Just as in Section 5.1, the standard deviations of the estimates were then compared to the ones given by the square roots of the diagonal elements in (25), see Figure 3. A comparison between Figures 2 and 3 illustrates that the variance of the measurement noise, used in the theoretic expression, should be lowered to give the right level of the accuracy of the estimates. After testing, it turned out that the variance should be decreased about 35%.

The strains, without added noise, in one of the sections are shown in Figure 4. In the figure we see that the wave is reflected a number of times at both ends of the bar specimen and also how the wave is damped.

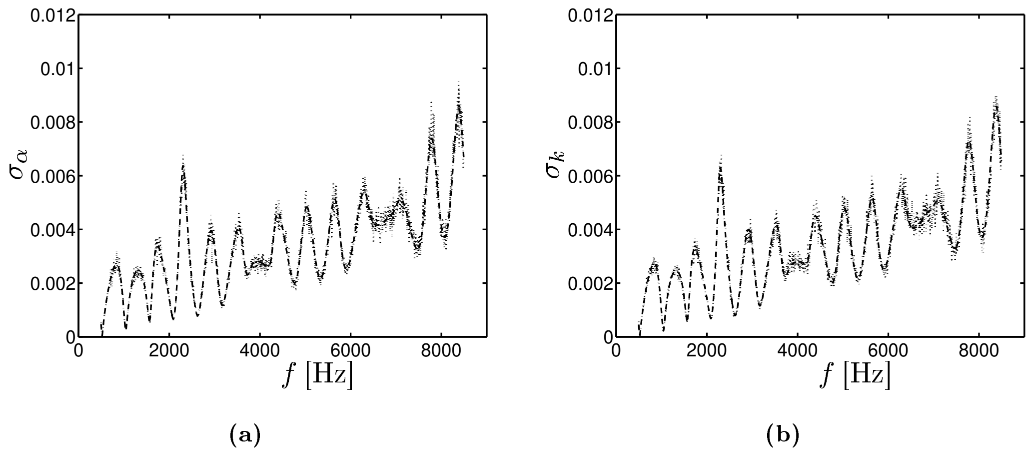

Figure 2: Numerical $(\cdots)$ and theoretical $(--)$ standard deviations for (a) $\gamma_r \equiv \alpha$ and (b) $\gamma_i \equiv k$ as functions of frequency. Noise was added to all strain data series, including the free-end strains.

In the simulations, the strain pulse at the right end of the bar specimen was chosen to give sufficient excitation at the frequencies of interest. The strain pulse, created in the time domain, is shown in Figure 5. In the experiments, the strain pulse is generated by a hammer, see Figure 1. It is not necessary to know its shape when using the non-parametric identification technique described in Section 3 . However, from studies of the strains in the section closest to the right end, the shape is quite well known. This knowledge is also used when constructing the strain pulse used in the simulations. The most important thing is not the shape of the pulse, but to choose a pulse that gives high enough energy for the frequencies considered.

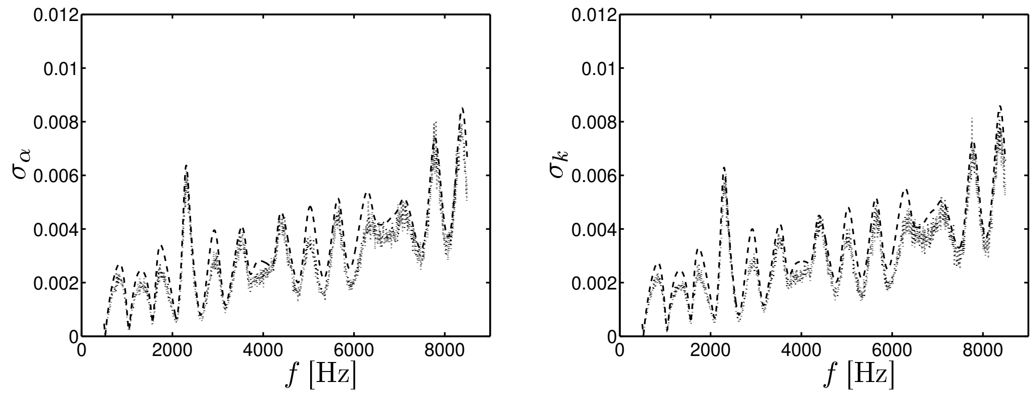

(a) **(b)**

Figure 3: Numerical $(\cdots)$ and theoretical $(--)$ standard deviations for (a) $\gamma_r \equiv \alpha$ and (b) $\gamma_i \equiv k$ as functions of frequency. No noise was added to the strain data series from the free end. After testing, it was found that the variance of the noise, used in the analytic expression, should be lowered about 35% to give the right level of the theoretical standard deviations.

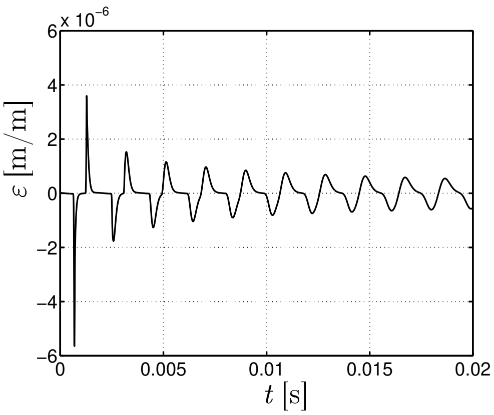

Figure 4: The simulated strains in a section as function of time.

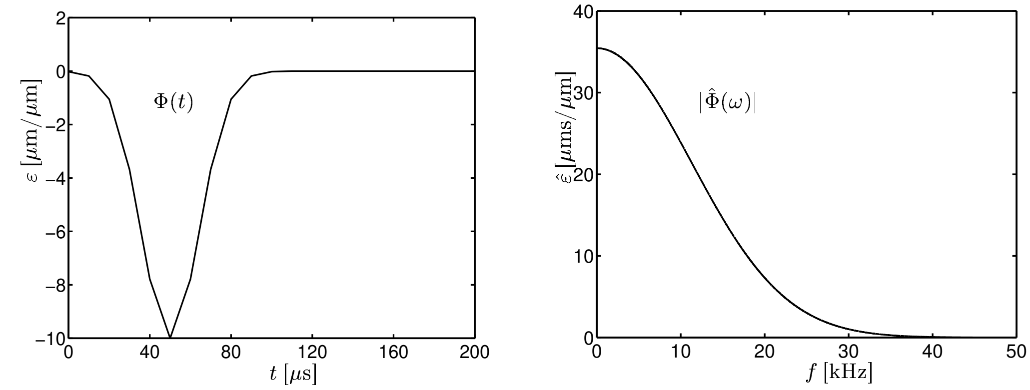

(a) **(b)**

Figure 5: (a) The strain pulse $\Phi(t)$ at the right end of the bar specimen, and (b) its Fourier transform $\hat{\Phi}(\omega)$.

6 Experiments

6.1 Data from experimental tests

In the previous section we saw that (25) was confirmed when simulated data were used. Naturally, it is even more important to find out if (25) is applicable also when real data are used. Therefore, ten experiments, as identical as possible, were carried out with a bar specimen made of plexiglass. Additional information about the experiments can be found in [4]. The standard deviations, taken as the square roots of the diagonal elements of (25), were evaluated with strain data from each of the ten experiments, and $\mathbf{g}_\infty(\omega_k)$ taken as the mean value of the ten identified wave propagation coefficients . The average of these standard deviations were taken as the theoretical standard deviations. This result was compared with the standard deviations of the ten identified wave propagation coefficients. The locations of the sensors and the length of the bar were the same as in the numerical example of Section 5. The number of data points were $N = 4096$ and the sampling interval $\Delta t = 20$ μs. The variance of the measurement noise was estimated to $\sigma^2 \approx 3.6 \cdot 10^{-14}$, see Section 6.2. To compensate for the noise-free data from the the free end, see the discussions in Sections 5.2 and 6.2, the variance $\sigma^2 \approx 2.1 \cdot 10^{-14}$ of the noise was used in (25). In Figure 6, the experimental and theoretical standard deviations are compared. In Figure 7, the mean values of the ten realisations, the mean values $\pm$ the standard deviations of the realisations, and the mean values $\pm$ the standard deviations from (25) are shown.

The complex modulus was obtained via (32). In Figure 8, the mean values of the ten realisations, the mean values $\pm$ the standard deviations of the realisations, and the mean values $\pm$ the standard deviations from (37) are shown.

6.2 Discussion

From Figures 6 and 7 we see that the theoretical expression (25) for the standard deviation is able to describe the experimental standard deviation with high enough accuracy. We see in Figure 6 that the standard deviations of the real and of the imaginary parts of the wave propagation coefficient are of the same order of magnitude. However, the order of the absolute values of the corresponding mean values differs considerable, see Figure 7. Hence, the relative expected accuracy of the estimated imaginary part is better than for the real part.

It is not possible to obtain estimates of good quality for all frequencies. A lower limit of useful frequencies can be estimated from the requirement that there must be sufficient variation of strain between the outermost sections x_1 and x_n. This implies wavelengths shorter than, say, ten times the distance between these sections. This corresponds to wavenumbers above 0.4 m^{-1} and frequencies above 100 to 200 Hz. An upper limit of useful frequencies can be estimated from the requirement of the one-dimensional model used that the wavelength must be at least, say, ten times the diameter of the bar specimen. This implies wavenumbers below 39 m^{-1} and frequencies below 14 kHz. Higher quality of the results is obtained if better excitation and thereby higher SNR can be achieved. Systematical errors, such as small errors in the sensor locations, also affect the estimates.

Several measurements were made in order to study the noise characteristics. In Figure 9, the power spectral density of one noise sequence is shown. The noise is very close to being white, which is an assumption in the analysis of the accuracy. The variance of the noise was estimated to be $\sigma^2 \approx 3.6 \cdot 10^{-14}$ from the relation

$$10 \cdot \log_{10} \sigma^2 = p, \tag{41}$$

where $p \approx -134.4$ dB is the power spectrum magnitude from Figure 9. The variance σ^2, used in the analytic expression for the expected accuracy, must be lowered to compensate for that one of the strain data series is noise free. This was discussed and illustrated with a Monte Carlo simulation in Section 5.2. After testing, it was found that a satisfying result is given with $\sigma^2 \approx 2.1 \cdot 10^{-14}$, a decrease with about 40%. The decrease is a little larger than what is expected from the numerical studies in Section 5.2.

The loss function $W\big(\gamma(\omega_k)\big)$ in (16) was minimised by using the simplex search method of [8]. A more time consuming grid search was carried out to check the results from the simplex method. To illustrate the difficulty of minimising (16), we consider the dimensionless measure

$$\mu\big(\gamma(\omega_k)\big) = \frac{\sqrt{W\big(\gamma(\omega_k)\big)}}{\|\hat{\varepsilon}(\omega_k)\|} \tag{42}$$

for different $\alpha(\omega_k)$ and $k(\omega_k)$, where

$$\gamma(\omega_k) = \gamma_r(\omega_k) + \mathrm{i}\gamma_i(\omega_k) = \alpha(\omega_k) + \mathrm{i}k(\omega_k). \tag{43}$$

For the material treated in this paper, (16) most often has a unique global minimum (and $\mu^{-1}\big(\gamma(\omega_k)\big)$ a unique global maximum) as for $f_k = 2$ kHz in Figure 10a and $f_k = 10$ kHz in Figure 10b. The global minimum may not always equal the solution searched for. In these rare cases the global minimum can be rejected by physical reasons, i. e. $\alpha(\omega_k)$ and $k(\omega_k)$ must be nonnegative and continuous functions.

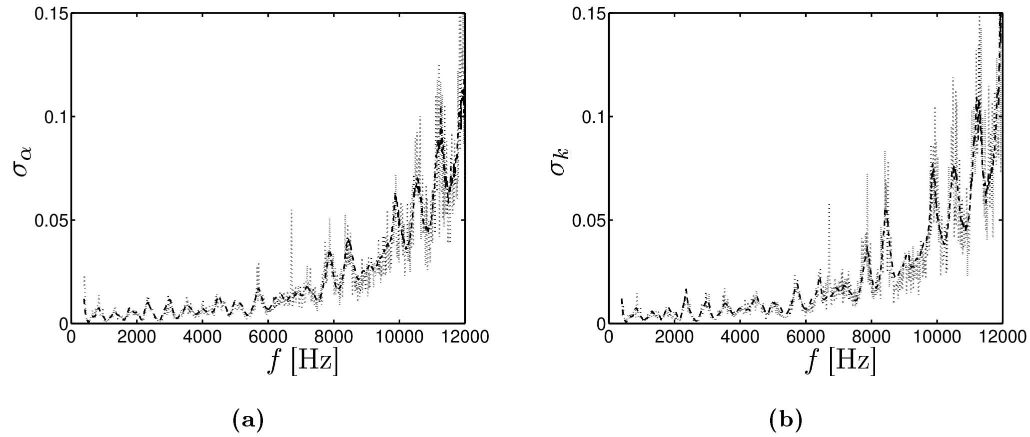

Figure 6: Experimental ($\cdots$) and theoretical ($--$) standard deviations for (a) $\gamma_r \equiv \alpha$ and (b) $\gamma_i \equiv k$ as functions of frequency.

7 Conclusions

It is of great importance to be able to fully characterise materials with viscoelastic behaviour in order to use them in engineering applications. A non-parametric identification of the frequency dependent wave propagation coefficient and the corresponding complex modulus was considered. A wave propagation experiment with an axially impacted bar specimen was carried out. Strains were measured at a number of sections in the bar. These strains were used together with the solution of a one-dimensional wave equation in the non-parametric identification. Asymptotic expressions for the accuracy of the estimated wave propagation coefficient and complex modulus, valid for high SNR:s, were derived. The standard deviations

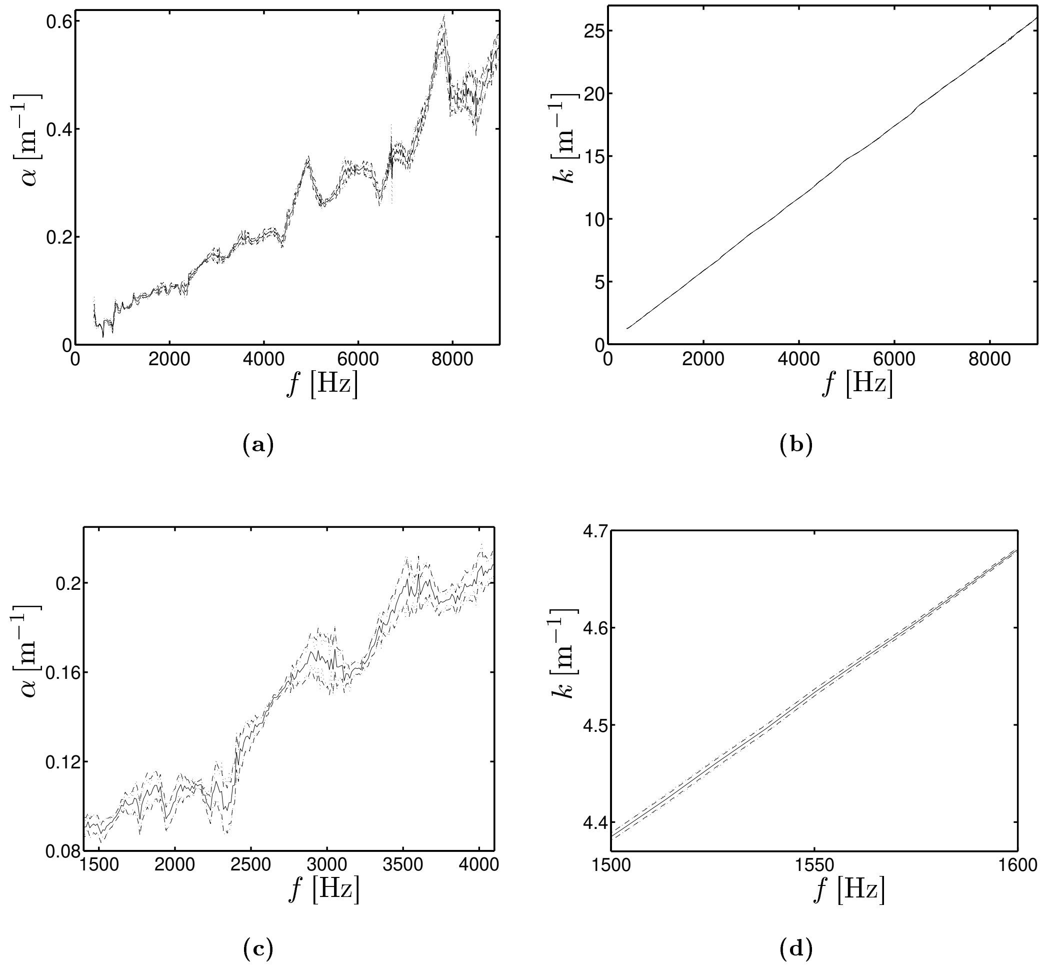

Figure 7: The mean values of the ten realisations (—), the mean values $\pm$ the standard deviations of the realisations $(\cdots)$ and the mean values $\pm$ the standard deviations from (25) with $(--)$ for (a) $\gamma_r \equiv \alpha$ and (b) $\gamma_i \equiv k$ as functions of frequency . Note that (c) and (d) show enlarged areas of (a) and (b), respectively, to illustrate the results with higher resolution.

given by the expression can be computed from a single realisation and the confidence in the estimated wave propagation coefficient and complex modulus can be expressed. The validity of the expression for the standard deviation of the estimated wave propagation coefficient was confirmed by a Monte Carlo simulation. Data were also taken from real experiments and it was concluded that the theoretical expression can describe the experimental standard deviations with high accuracy. Identification of a parametric model is under investigation.

Acknowledgments

The authors want to thank Dr. L. Abrahamsson, Dr. B. Carlsson and Prof. B. Lundberg for their cooperation and valuable comments on the paper.

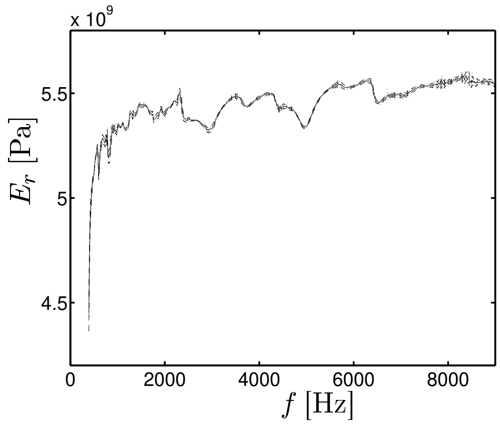

(a)

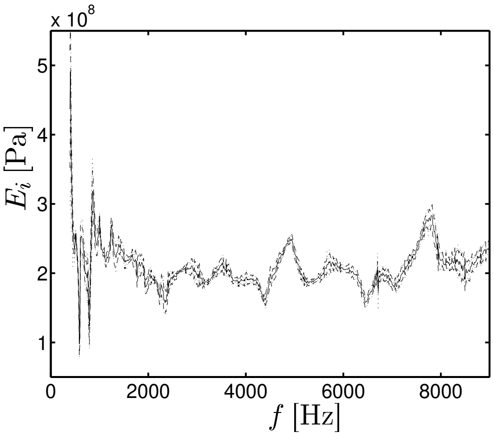

(b)

Figure 8: The mean values of the ten realisations (—), the mean values ± the standard deviations of the realisations (···) and the mean values ± the standard deviations from (37) with (−−) for (a) E_r and (b) E_i as functions of frequency.

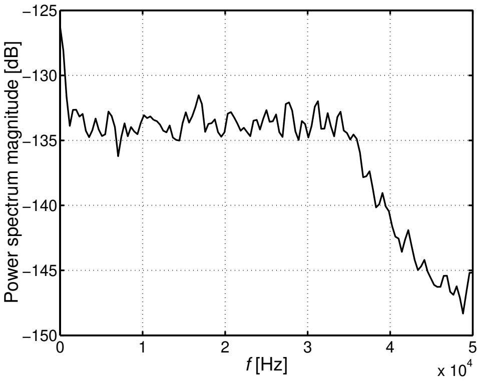

Figure 9: The power spectral density estimate of a measurement noise sequence as function of frequency. An analog lowpass filtering with cut-off frequency 35 kHz (70% of half the sampling frequency) has been made.

References

[1] R. H. Blanc. Transient wave propagation methods for determining the viscoelastic properties of solids. *Journal of Applied Mechanics*, 60:763–768, 1993.

[2] J. L. Buchanan. Numerical solution for the dynamic moduli of a viscoelastic bar. *J. Acoust. Soc. Am.*, 81(6):1775–1786, June 1987.

[3] G. H. Golub and V. Pereyra. The differentiation of pseudo-inverses and nonlinear least squares problems whose variables separate. *SIAM J. Numer. Anal.*, 10(2):413–432, 1973.

[4] L. Hillström, M. Mossberg, and B. Lundberg. Identification of complex modulus from measured strains on an axially impacted bar using least squares. To be published in *Journal of Sound and Vibration*, March 2000.

[5] A. J. Hull. An inverse method to measure the axial modulus of composite materials under tension. *Journal of Sound and Vibration*, 195(4):545–551, 1996.

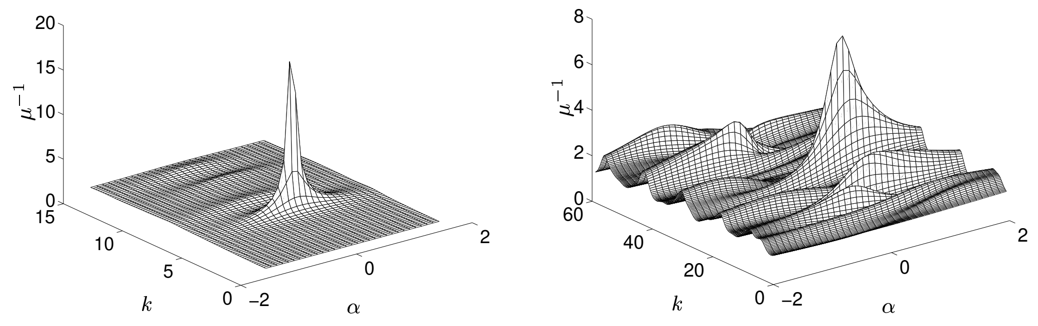

(a) **(b)**

Figure 10: The dimensionless measure $\mu^{-1}(\gamma(\omega_k))$ as a function of $\alpha(\omega_k)$ and $k(\omega_k)$ for (a) $f_k = 2$ kHz and (b) $f_k = 10$ kHz.

[6] B. Lundberg and R. H. Blanc. Determination of mechanical material properties from the two-point response of an impacted linearly viscoelastic rod specimen. *Journal of Sound and Vibration*, 126(1):97–108, 1988.

[7] B. Lundberg and S. Ödeen. *In situ* determination of the complex modulus from strain measurements on an impacted structure. *Journal of Sound and Vibration*, 167(3):413–419, 1993.

[8] J. A. Nelder and R. Mead. A simplex method for function minimization. *Computer Journal*, 7:308–313, 1965.

[9] T. Söderström and P. Stoica. *System Identification.* Prentice–Hall International, Hemel Hempstead, United Kingdom, 1989.

[10] M. Soula, T. Vinh, Y. Chevalier, T. Beda, and C. Esteoule. Measurements of isothermal complex moduli of viscoelastic materials over a large range of frequencies. *Journal of Sound and Vibration*, 205(2):167–184, 1997.

[11] G. W. Stewart. On the pertutbation of pseudo-inverses, projections, and linear least squares problems. *SIAM Review*, 19:634–662, 1977.

[12] C. Zener. *Elasticity and Anelasticity of Metals.* University of Chicago Press, IL, USA, 1948.

A Description of the wave propagation

The most basic model of one-dimensional longitudinal vibrations of a slender rod can be written

$$\rho \frac{\partial v(x,t)}{\partial t} = \frac{\partial \sigma(x,t)}{\partial x}, \tag{44}$$

$$\frac{\partial \varepsilon(x,t)}{\partial t} = \frac{\partial v(x,t)}{\partial x}, \tag{45}$$

where ρ is the density and $v(x,t)$, $\sigma(x,t)$ and $\varepsilon(x,t)$ are the particle velocity, stress and strain at position x at time t. Differentiation of both equations with respect to t gives

$$\rho \frac{\partial^2 \varepsilon(x,t)}{\partial t^2} = \frac{\partial^2 \sigma(x,t)}{\partial x^2}. \tag{46}$$

A general form of a constitutive equation connecting stress and strain for a viscoelastic material is

$$A(p)\sigma(x,t) = B(p)\varepsilon(x,t), \tag{47}$$

where $A(p)$ and $B(p)$ are polynomials in $p = \frac{d}{dt}$. Fourier transformation of (47) gives

$$\hat{\sigma}(x,\omega) = \frac{B(\mathrm{i}\omega)}{A(\mathrm{i}\omega)}\hat{\varepsilon}(x,\omega) \triangleq E(\omega)\hat{\varepsilon}(x,\omega), \tag{48}$$

where ω is the angular frequency and $E(\omega)$ is the complex modulus. The convolution theorem gives

$$\sigma(x,t) = \mathcal{F}^{-1}\{E(\omega)\} * \varepsilon(x,t), \tag{49}$$

where $\mathcal{F}^{-1}$ denotes inverse Fourier transformation and $*$ is the convolution operator. Finally, Equations (46) and (49) give

$$\mathcal{F}^{-1}\left\{\frac{E(\omega)}{\rho}\right\} * \frac{\partial^2 \varepsilon(x,t)}{\partial x^2} = \frac{\partial^2 \varepsilon(x,t)}{\partial t^2}. \tag{50}$$

B Derivation of gradient vector and Hessian matrix of V

The loss function (16) can be evaluated as

$$W(\gamma) = \left\|\hat{\boldsymbol{\varepsilon}} - \mathbf{A}\mathbf{A}^{\dagger}\hat{\boldsymbol{\varepsilon}}\right\|^2 = \left\|(\mathbf{I} - \mathbf{A}\mathbf{A}^{\dagger})\hat{\boldsymbol{\varepsilon}}\right\|^2 = \hat{\boldsymbol{\varepsilon}}^*(\mathbf{I} - \mathbf{A}\mathbf{A}^{\dagger})\hat{\boldsymbol{\varepsilon}} \tag{51}$$

where $\gamma = \gamma(\omega_k)$, $\hat{\boldsymbol{\varepsilon}} = \hat{\boldsymbol{\varepsilon}}(\omega_k)$ and $\mathbf{A} = \mathbf{A}(\gamma)$. Consider, as before, $W(\gamma)$ as a function of two real-valued variables, $W(\gamma) = V(\mathbf{g})$, where $\mathbf{g}$ is given by (19). The gradient vector

$$\mathbf{V}'(\mathbf{g}) = \begin{bmatrix} \frac{\partial V}{\partial \gamma_r} & \frac{\partial V}{\partial \gamma_i} \end{bmatrix}^T \tag{52}$$

and the Hessian matrix

$$\mathbf{V}''(\mathbf{g}) = \begin{bmatrix} \frac{\partial^2 V}{\partial \gamma_r^2} & \frac{\partial^2 V}{\partial \gamma_i \partial \gamma_r} \\ \frac{\partial^2 V}{\partial \gamma_r \partial \gamma_i} & \frac{\partial^2 V}{\partial \gamma_i^2} \end{bmatrix} \tag{53}$$

will be derived. Derivatives of orthogonal projectors and pseudoinverses were considered in [3, 11]. The short hand notations

$$\mathbf{A}_r = \frac{\partial \mathbf{A}}{\partial \gamma_r}, \qquad \mathbf{A}_i = \frac{\partial \mathbf{A}}{\partial \gamma_i} \tag{54}$$

and

$$\mathbf{A}_{rr} = \frac{\partial^2 \mathbf{A}}{\partial \gamma_r^2}, \quad \mathbf{A}_{ri} = \frac{\partial^2 \mathbf{A}}{\partial \gamma_i \gamma_r}, \quad \mathbf{A}_{ii} = \frac{\partial^2 \mathbf{A}}{\partial \gamma_i^2}, \quad \mathbf{A}_{ir} = \frac{\partial^2 \mathbf{A}}{\partial \gamma_r \gamma_i} = \mathbf{A}_{ri}. \tag{55}$$

will be convenient to use. Differentiation of V with respect to γ_r gives

$$
\begin{aligned}
\frac{\partial V(\mathbf{g})}{\partial \gamma_r} &= \hat{\varepsilon}^* \big(-\mathbf{A}_r \mathbf{A}^\dagger - \mathbf{A}(\mathbf{A}^\dagger)_r \big) \hat{\varepsilon} \\
&= \hat{\varepsilon}^* \big(-\mathbf{A}_r \mathbf{A}^\dagger + \mathbf{A}[\mathbf{A}^*\mathbf{A}]^{-1}(\mathbf{A}_r^*\mathbf{A} + \mathbf{A}^*\mathbf{A}_r)[\mathbf{A}^*\mathbf{A}]^{-1}\mathbf{A}^* \\
&\quad - \mathbf{A}[\mathbf{A}^*\mathbf{A}]^{-1}\mathbf{A}_r^* \big) \hat{\varepsilon} \\
&= \hat{\varepsilon}^* \big(-\mathbf{A}_r \mathbf{A}^\dagger + \mathbf{A}^{\dagger *}\mathbf{A}_r^*\mathbf{A}^{\dagger *}\mathbf{A}^* + \mathbf{A}\mathbf{A}^\dagger \mathbf{A}_r \mathbf{A}^\dagger - \mathbf{A}^{\dagger *}\mathbf{A}_r^* \big) \hat{\varepsilon} \\
&= \hat{\varepsilon}^* \big((\mathbf{A}\mathbf{A}^\dagger - \mathbf{I})\mathbf{A}_r \mathbf{A}^\dagger + (\dots)^* \big) \hat{\varepsilon} \\
&= \hat{\varepsilon}^* \big(-\boldsymbol{\Pi}^\perp \mathbf{A}_r \mathbf{A}^\dagger + (\dots)^* \big) \hat{\varepsilon},
\end{aligned} \tag{56}
$$

where

$$
\boldsymbol{\Pi}^\perp = \mathbf{I} - \mathbf{A}\mathbf{A}^\dagger \tag{57}
$$

is the orthogonal projection onto the null space of $\mathbf{A}^*$. The notation $(\dots)^*$ means that the same expression appears again with complex conjugate and transpose. Similarly to (56) we get that

$$
\frac{\partial V(\mathbf{g})}{\partial \gamma_i} = \hat{\varepsilon}^* \big(-\boldsymbol{\Pi}^\perp \mathbf{A}_i \mathbf{A}^\dagger + (\dots)^* \big) \hat{\varepsilon}. \tag{58}
$$

When (56) and (58) are evaluated for $\mathbf{g} = \mathbf{g}_\infty$, we write

$$
\frac{\partial V(\mathbf{g}_\infty)}{\partial \gamma_r} = \hat{\varepsilon}^* \mathbf{P}_r \hat{\varepsilon}, \tag{59}
$$

$$
\frac{\partial V(\mathbf{g}_\infty)}{\partial \gamma_i} = \hat{\varepsilon}^* \mathbf{P}_i \hat{\varepsilon}, \tag{60}
$$

where

$$
\mathbf{P}_r = -\boldsymbol{\Pi}^\perp \mathbf{A}_r \mathbf{A}^\dagger + (\dots)^*, \tag{61}
$$

$$
\mathbf{P}_i = -\boldsymbol{\Pi}^\perp \mathbf{A}_i \mathbf{A}^\dagger + (\dots)^*. \tag{62}
$$

Note that all matrices are evaluated for $\mathbf{g} = \mathbf{g}_\infty$ in the definitions (61) and (62), and that $\nexists\ \mathbf{P} = \mathbf{P}_r + \mathrm{i}\mathbf{P}_i$. A straightforward but tedious differentiation of (56) with respect to γ_i gives

$$
\begin{aligned}
\frac{\partial^2 V}{\partial \gamma_i \partial \gamma_r} &= \hat{\varepsilon}^* \big(\boldsymbol{\Pi}^\perp \mathbf{A}_i \mathbf{A}^\dagger \mathbf{A}_r \mathbf{A}^\dagger + \mathbf{A}^{\dagger *}\mathbf{A}_i^* \boldsymbol{\Pi}^\perp \mathbf{A}_r \mathbf{A}^\dagger - \boldsymbol{\Pi}^\perp \mathbf{A}_{ri} \mathbf{A}^\dagger \\
&\quad - \boldsymbol{\Pi}^\perp \mathbf{A}_r [\mathbf{A}^*\mathbf{A}]^{-1} \mathbf{A}_i^* \boldsymbol{\Pi}^\perp + \boldsymbol{\Pi}^\perp \mathbf{A}_r \mathbf{A}^\dagger \mathbf{A}_i \mathbf{A}^\dagger + (\dots)^* \big) \hat{\varepsilon}.
\end{aligned} \tag{63}
$$

The other three elements in the Hessian matrix (53) can be obtained from (63) in the same way as (58) was obtained from (56). When the SNR tends to infinity and the elements of the Hessian matrix are evaluated for $\mathbf{g} = \mathbf{g}_\infty$, see (24), we write

$$
\mathbf{H} = \begin{bmatrix} \hat{\boldsymbol{\epsilon}}^* \mathbf{B}_{rr} \hat{\boldsymbol{\epsilon}} & \hat{\boldsymbol{\epsilon}}^* \mathbf{B}_{ri} \hat{\boldsymbol{\epsilon}} \\ \hat{\boldsymbol{\epsilon}}^* \mathbf{B}_{ir} \hat{\boldsymbol{\epsilon}} & \hat{\boldsymbol{\epsilon}}^* \mathbf{B}_{ii} \hat{\boldsymbol{\epsilon}} \end{bmatrix}, \tag{64}
$$

where

$$
\begin{aligned}
\mathbf{B}_{rr} &= 2\boldsymbol{\Pi}^\perp \mathbf{A}_r \mathbf{A}^\dagger \mathbf{A}_r \mathbf{A}^\dagger + \mathbf{A}^{\dagger *}\mathbf{A}_r^* \boldsymbol{\Pi}^\perp \mathbf{A}_r \mathbf{A}^\dagger - \boldsymbol{\Pi}^\perp \mathbf{A}_{rr} \mathbf{A}^\dagger \\
&\quad - \boldsymbol{\Pi}^\perp \mathbf{A}_r [\mathbf{A}^*\mathbf{A}]^{-1} \mathbf{A}_r^* \boldsymbol{\Pi}^\perp + (\dots)^*, \qquad (65) \\
\mathbf{B}_{ri} &= \boldsymbol{\Pi}^\perp \mathbf{A}_i \mathbf{A}^\dagger \mathbf{A}_r \mathbf{A}^\dagger + \mathbf{A}^{\dagger *}\mathbf{A}_i^* \boldsymbol{\Pi}^\perp \mathbf{A}_r \mathbf{A}^\dagger - \boldsymbol{\Pi}^\perp \mathbf{A}_{ri} \mathbf{A}^\dagger \\
&\quad - \boldsymbol{\Pi}^\perp \mathbf{A}_r [\mathbf{A}^*\mathbf{A}]^{-1} \mathbf{A}_i^* \boldsymbol{\Pi}^\perp + \boldsymbol{\Pi}^\perp \mathbf{A}_r \mathbf{A}^\dagger \mathbf{A}_i \mathbf{A}^\dagger + (\dots)^*, \qquad (66) \\
\mathbf{B}_{ir} &= \mathbf{B}_{ri}, \qquad (67) \\
\mathbf{B}_{ii} &= 2\boldsymbol{\Pi}^\perp \mathbf{A}_i \mathbf{A}^\dagger \mathbf{A}_i \mathbf{A}^\dagger + \mathbf{A}^{\dagger *}\mathbf{A}_i^* \boldsymbol{\Pi}^\perp \mathbf{A}_i \mathbf{A}^\dagger - \boldsymbol{\Pi}^\perp \mathbf{A}_{ii} \mathbf{A}^\dagger \\
&\quad - \boldsymbol{\Pi}^\perp \mathbf{A}_i [\mathbf{A}^*\mathbf{A}]^{-1} \mathbf{A}_i^* \boldsymbol{\Pi}^\perp + (\dots)^*. \qquad (68)
\end{aligned}
$$

Note that all matrices are evaluated for $\mathbf{g} = \mathbf{g}_\infty$ in the definitions (65)–(68).

In Lemma 2 we will state some useful results for the matrices $\mathbf{P}_r$ and $\mathbf{P}_i$ introduced in (61) and (62).

Lemma 2 *For the matrices $\mathbf{P}_r$ and $\mathbf{P}_i$ defined in (61) and (62) it holds that*

$$\mathrm{tr}\{\mathbf{P}_r\} = 0, \tag{69}$$
$$\mathrm{tr}\{\mathbf{P}_i\} = 0, \tag{70}$$
$$\mathrm{tr}\{\mathbf{P}_r\mathbf{P}_i\} = 0, \tag{71}$$
$$\mathbf{P}_r\mathbf{P}_i + \mathbf{P}_i\mathbf{P}_r = \mathbf{0}. \tag{72}$$

□

Proof To prove (69) it is sufficient to show that

$$\mathrm{tr}\{\mathbf{\Pi}^\perp\mathbf{A}_r\mathbf{A}^\dagger\} = 0. \tag{73}$$

We have that

$$\begin{aligned}\mathrm{tr}\{\mathbf{\Pi}^\perp\mathbf{A}_r\mathbf{A}^\dagger\} &= \mathrm{tr}\{(\mathbf{I} - \mathbf{A}\mathbf{A}^\dagger)\mathbf{A}_r\mathbf{A}^\dagger\} = \mathrm{tr}\{\mathbf{A}_r\mathbf{A}^\dagger\} - \mathrm{tr}\{\mathbf{A}^\dagger\mathbf{A}_r\underbrace{\mathbf{A}^\dagger\mathbf{A}}_{=\mathbf{I}}\} \\ &= \mathrm{tr}\{\mathbf{A}_r\mathbf{A}^\dagger\} - \mathrm{tr}\{\mathbf{A}_r\mathbf{A}^\dagger\} = 0,\end{aligned} \tag{74}$$

where we have used that for matrices $\mathbf{X}$ and $\mathbf{Y}$ of compatible dimensions

$$\mathrm{tr}\{\mathbf{X}\mathbf{Y}\} = \mathrm{tr}\{\mathbf{Y}\mathbf{X}\}. \tag{75}$$

Relation (69) is thereby proved. The proof of (70) follows in the same way. In order to prove (72), we use that $\mathbf{A}^\dagger\mathbf{\Pi}^\perp = \mathbf{0}$ and $\mathbf{\Pi}^{\perp *} = \mathbf{\Pi}^\perp$ to get

$$\begin{aligned}\mathbf{P}_r\mathbf{P}_i + \mathbf{P}_i\mathbf{P}_r = {}& \mathbf{\Pi}^\perp\mathbf{A}_r\mathbf{A}^\dagger\mathbf{A}^{\dagger *}\mathbf{A}_i^*\mathbf{\Pi}^\perp + \mathbf{A}^{\dagger *}\mathbf{A}_r^*\mathbf{\Pi}^{\perp 2}\mathbf{A}_i\mathbf{A}^\dagger \\ &+ \mathbf{\Pi}^\perp\mathbf{A}_i\mathbf{A}^\dagger\mathbf{A}^{\dagger *}\mathbf{A}_r^*\mathbf{\Pi}^\perp + \mathbf{A}^{\dagger *}\mathbf{A}_i^*\mathbf{\Pi}^{\perp 2}\mathbf{A}_r\mathbf{A}^\dagger.\end{aligned} \tag{76}$$

Since $\mathbf{A}_i = \mathrm{i}\mathbf{A}_r$, the right hand side will vanish, and (72) is proved. Relation (71) follows directly from (72) and (75). □

C Proof of Lemma 1

In this section we will prove that the elements of $\mathbf{G}(\omega_a, \omega_b)$, defined in (26), are given by (30) and (31), when the measurements are affected by spatially and temporally white Gaussian noise. The derivation will be made only for the elements $\mathbf{G}_{12}(\omega_a, \omega_b)$ and $\mathbf{G}_{11}(\omega_a, \omega_b)$, since the other two elements are easily obtained from these results. We have that

$$\mathbf{G}_{12}(\omega_a, \omega_b) = \mathrm{E}\left\{\frac{\partial V\big(\mathbf{g}_\infty(\omega_a)\big)}{\partial \gamma_r} \cdot \frac{\partial V\big(\mathbf{g}_\infty(\omega_b)\big)}{\partial \gamma_i}\right\}. \tag{77}$$

In Appendix B, equations (59) and (60), it was shown that

$$\frac{\partial V\big(\mathbf{g}_\infty(\omega_k)\big)}{\partial \gamma_r} = \hat{\varepsilon}^*(\omega_k)\mathbf{P}_r(\omega_k)\hat{\varepsilon}(\omega_k), \tag{78}$$
$$\frac{\partial V\big(\mathbf{g}_\infty(\omega_k)\big)}{\partial \gamma_i} = \hat{\varepsilon}^*(\omega_k)\mathbf{P}_i(\omega_k)\hat{\varepsilon}(\omega_k), \tag{79}$$

with $\mathbf{P}_r(\omega_k)$ and $\mathbf{P}_r(\omega_k)$ given by (61) and (62). From the definition of the discrete Fourier transform, we get that

$$\hat{\boldsymbol{\varepsilon}}(\omega_k) = \sum_{l=1}^{N} \varphi^{k(l-1)} \boldsymbol{\varepsilon}(t_l), \tag{80}$$

where

$$\varphi = e^{i\frac{2\pi}{N}}, \qquad \boldsymbol{\varepsilon}(t_l) = \begin{bmatrix} \varepsilon_1(t_l) \\ \vdots \\ \varepsilon_n(t_l) \end{bmatrix}. \tag{81}$$

We use (78), (79) and (80) to get

$$\begin{aligned} \mathbf{G}_{12}(\omega_a, \omega_b) &= \mathrm{E}\Big\{ \hat{\boldsymbol{\varepsilon}}^*(\omega_a) \mathbf{P}_r(\omega_a) \hat{\boldsymbol{\varepsilon}}(\omega_a) \hat{\boldsymbol{\varepsilon}}^*(\omega_b) \mathbf{P}_i(\omega_b) \hat{\boldsymbol{\varepsilon}}(\omega_b) \Big\} \\ &= \sum_{l_1=1}^{N} \sum_{l_2=1}^{N} \sum_{l_3=1}^{N} \sum_{l_4=1}^{N} \mathrm{E}\Big\{ \boldsymbol{\varepsilon}^T(t_{l_1}) \varphi^{a(1-l_1)} \mathbf{P}_r(\omega_a) \varphi^{a(l_2-1)} \boldsymbol{\varepsilon}(t_{l_2}) \\ &\quad \times \boldsymbol{\varepsilon}^T(t_{l_3}) \varphi^{b(1-l_3)} \mathbf{P}_i(\omega_b) \varphi^{b(l_4-1)} \boldsymbol{\varepsilon}(t_{l_4}) \Big\} \\ &\triangleq \sum_{l_1=1}^{N} \sum_{l_2=1}^{N} \sum_{l_3=1}^{N} \sum_{l_4=1}^{N} \mathrm{E}\Big\{ \boldsymbol{\varepsilon}_{l_1}^T \mathbf{C}_{l_1,l_2,r}(\omega_a) \boldsymbol{\varepsilon}_{l_2} \boldsymbol{\varepsilon}_{l_3}^T \mathbf{C}_{l_3,l_4,i}(\omega_b) \boldsymbol{\varepsilon}_{l_4} \Big\}, \end{aligned} \tag{82}$$

where shorter notations have been introduced as

$$\boldsymbol{\varepsilon}_{l_k} = \boldsymbol{\varepsilon}(t_{l_k}), \qquad k = 1, \ldots, 4 \tag{83}$$

$$\mathbf{C}_{l_1,l_2,r}(\omega_k) = \varphi^{k(l_2-l_1)} \mathbf{P}_r(\omega_k), \tag{84}$$

$$\mathbf{C}_{l_1,l_2,i}(\omega_k) = \varphi^{k(l_2-l_1)} \mathbf{P}_i(\omega_k). \tag{85}$$

Substitute (18) in (82) and note that the first and third moments of $\mathbf{v}(t_k)$ are zero as they are Gaussian variables,

$$\begin{aligned} \mathbf{G}_{12}(\omega_a, \omega_b) = \sum_{l_1=1}^{N} \sum_{l_2=1}^{N} \sum_{l_3=1}^{N} \sum_{l_4=1}^{N} \mathrm{E}\Big\{ & \boldsymbol{\epsilon}_{l_1}^T \mathbf{C}_{l_1,l_2,r}(\omega_a) \boldsymbol{\epsilon}_{l_2} \boldsymbol{\epsilon}_{l_3}^T \mathbf{C}_{l_3,l_4,i}(\omega_b) \boldsymbol{\epsilon}_{l_4} \\ & + \mathbf{v}_{l_1}^T \mathbf{C}_{l_1,l_2,r}(\omega_a) \mathbf{v}_{l_2} \mathbf{v}_{l_3}^T \mathbf{C}_{l_3,l_4,i}(\omega_b) \mathbf{v}_{l_4} + \boldsymbol{\epsilon}_{l_1}^T \mathbf{C}_{l_1,l_2,r}(\omega_a) \mathbf{v}_{l_2} \mathbf{v}_{l_3}^T \mathbf{C}_{l_3,l_4,i}(\omega_b) \boldsymbol{\epsilon}_{l_4} \\ & + \mathbf{v}_{l_1}^T \mathbf{C}_{l_1,l_2,r}(\omega_a) \boldsymbol{\epsilon}_{l_2} \mathbf{v}_{l_3}^T \mathbf{C}_{l_3,l_4,i}(\omega_b) \boldsymbol{\epsilon}_{l_4} + \mathbf{v}_{l_1}^T \mathbf{C}_{l_1,l_2,r}(\omega_a) \mathbf{v}_{l_2} \boldsymbol{\epsilon}_{l_3}^T \mathbf{C}_{l_3,l_4,i}(\omega_b) \boldsymbol{\epsilon}_{l_4} \\ & + \boldsymbol{\epsilon}_{l_1}^T \mathbf{C}_{l_1,l_2,r}(\omega_a) \boldsymbol{\epsilon}_{l_2} \mathbf{v}_{l_3}^T \mathbf{C}_{l_3,l_4,i}(\omega_b) \mathbf{v}_{l_4} + \boldsymbol{\epsilon}_{l_1}^T \mathbf{C}_{l_1,l_2,r}(\omega_a) \mathbf{v}_{l_2} \boldsymbol{\epsilon}_{l_3}^T \mathbf{C}_{l_3,l_4,i}(\omega_b) \mathbf{v}_{l_4} \\ & + \mathbf{v}_{l_1}^T \mathbf{C}_{l_1,l_2,r}(\omega_a) \boldsymbol{\epsilon}_{l_2} \boldsymbol{\epsilon}_{l_3}^T \mathbf{C}_{l_3,l_4,i}(\omega_b) \mathbf{v}_{l_4} \Big\}. \end{aligned} \tag{86}$$

From (20) and (21) it holds that $\mathbf{V}'\big(\mathbf{g}_\infty(\omega)\big) \to 0$ when $\sigma^2 \to 0$. Equations (78) and (79) then gives that

$$\sum_{l_1=1}^{N} \sum_{l_2=1}^{N} \boldsymbol{\epsilon}_{l_1}^T \mathbf{C}_{l_1,l_2,r}(\omega_k) \boldsymbol{\epsilon}_{l_2} = 0, \tag{87}$$

$$\sum_{l_3=1}^{N} \sum_{l_4=1}^{N} \boldsymbol{\epsilon}_{l_3}^T \mathbf{C}_{l_3,l_4,i}(\omega_k) \boldsymbol{\epsilon}_{l_4} = 0. \tag{88}$$

Several terms in (86) therefore disappear, and we get

$$\begin{aligned}\mathbf{G}_{12}(\omega_a,\omega_b) = \sum_{l_1=1}^{N}\sum_{l_2=1}^{N}\sum_{l_3=1}^{N}\sum_{l_4=1}^{N} \mathrm{E}\Big\{&\mathbf{v}_{l_1}^T\mathbf{C}_{l_1,l_2,r}(\omega_a)\mathbf{v}_{l_2}\mathbf{v}_{l_3}^T\mathbf{C}_{l_3,l_4,i}(\omega_b)\mathbf{v}_{l_4}\\ &+\boldsymbol{\epsilon}_{l_1}^T\mathbf{C}_{l_1,l_2,r}(\omega_a)\mathbf{v}_{l_2}\mathbf{v}_{l_3}^T\mathbf{C}_{l_3,l_4,i}(\omega_b)\boldsymbol{\epsilon}_{l_4}+\mathbf{v}_{l_1}^T\mathbf{C}_{l_1,l_2,r}(\omega_a)\boldsymbol{\epsilon}_{l_2}\mathbf{v}_{l_3}^T\mathbf{C}_{l_3,l_4,i}(\omega_b)\boldsymbol{\epsilon}_{l_4}\\ &+\boldsymbol{\epsilon}_{l_1}^T\mathbf{C}_{l_1,l_2,r}(\omega_a)\mathbf{v}_{l_2}\boldsymbol{\epsilon}_{l_3}^T\mathbf{C}_{l_3,l_4,i}(\omega_b)\mathbf{v}_{l_4}+\mathbf{v}_{l_1}^T\mathbf{C}_{l_1,l_2,r}(\omega_a)\boldsymbol{\epsilon}_{l_2}\boldsymbol{\epsilon}_{l_3}^T\mathbf{C}_{l_3,l_4,i}(\omega_b)\mathbf{v}_{l_4}\Big\}.\end{aligned} \tag{89}$$

To evaluate the terms in the quadripel sum, we use that for vectors $\mathbf{x}$ and $\mathbf{y}$ it holds that

$$\mathbf{y}^T\mathbf{x} = \mathrm{tr}\{\mathbf{x}\mathbf{y}^T\}. \tag{90}$$

We also rewrite the first term in (89) as [9]

$$\begin{aligned}\mathrm{E}\Big\{\mathbf{v}_{l_1}^T\mathbf{C}_{l_1,l_2,r}(\omega_a)\mathbf{v}_{l_2}\mathbf{v}_{l_3}^T\mathbf{C}_{l_3,l_4,i}(\omega_b)\mathbf{v}_{l_4}\Big\} = {}&\mathrm{E}\Big\{\mathbf{v}_{l_1}^T\mathbf{C}_{l_1,l_2,r}(\omega_a)\mathbf{v}_{l_2}\Big\}\mathrm{E}\Big\{\mathbf{v}_{l_3}^T\mathbf{C}_{l_3,l_4,i}(\omega_b)\mathbf{v}_{l_4}\Big\}\\ &+\mathrm{E}\Big\{\mathbf{v}_{l_2}^T\mathbf{C}_{l_1,l_2,r}^T(\omega_a)\mathrm{E}\{\mathbf{v}_{l_1}\mathbf{v}_{l_3}^T\}\mathbf{C}_{l_3,l_4,i}(\omega_b)\mathbf{v}_{l_4}\Big\}\\ &+\mathrm{E}\Big\{\mathbf{v}_{l_1}^T\mathbf{C}_{l_1,l_2,r}(\omega_a)\mathrm{E}\{\mathbf{v}_{l_2}\mathbf{v}_{l_3}^T\}\mathbf{C}_{l_3,l_4,i}(\omega_b)\mathbf{v}_{l_4}\Big\}.\end{aligned} \tag{91}$$

This gives that (89) can be rewritten as

$$\begin{aligned}\mathbf{G}_{12}(\omega_a,\omega_b) = \sum_{l_1=1}^{N}\sum_{l_2=1}^{N}\sum_{l_3=1}^{N}\sum_{l_4=1}^{N}\Big[&\delta_{l_1,l_2}\delta_{l_3,l_4}\sigma^4\mathrm{tr}\{\mathbf{C}_{l_1,l_2,r}(\omega_a)\}\mathrm{tr}\{\mathbf{C}_{l_3,l_4,i}(\omega_b)\}\\ &+\delta_{l_1,l_3}\delta_{l_2,l_4}\sigma^4\mathrm{tr}\{\mathbf{C}_{l_1,l_2,r}^T(\omega_a)\mathbf{C}_{l_3,l_4,i}(\omega_b)\}+\delta_{l_1,l_4}\delta_{l_2,l_3}\sigma^4\mathrm{tr}\{\mathbf{C}_{l_1,l_2,r}(\omega_a)\mathbf{C}_{l_3,l_4,i}(\omega_b)\}\\ &+\delta_{l_2,l_3}\sigma^2\boldsymbol{\epsilon}_{l_1}^T\mathbf{C}_{l_1,l_2,r}(\omega_a)\mathbf{C}_{l_3,l_4,i}(\omega_b)\boldsymbol{\epsilon}_{l_4}+\delta_{l_1,l_3}\sigma^2\boldsymbol{\epsilon}_{l_2}^T\mathbf{C}_{l_1,l_2,r}^T(\omega_a)\mathbf{C}_{l_3,l_4,i}(\omega_b)\boldsymbol{\epsilon}_{l_4}\\ &+\delta_{l_2,l_4}\sigma^2\boldsymbol{\epsilon}_{l_3}^T\mathbf{C}_{l_3,l_4,i}(\omega_b)\mathbf{C}_{l_1,l_2,r}^T(\omega_a)\boldsymbol{\epsilon}_{l_1}+\delta_{l_1,l_4}\sigma^2\boldsymbol{\epsilon}_{l_3}^T\mathbf{C}_{l_3,l_4,i}(\omega_b)\mathbf{C}_{l_1,l_2,r}(\omega_a)\boldsymbol{\epsilon}_{l_2}\Big].\end{aligned} \tag{92}$$

We denote the seven terms in (92) by T_1–T_7 and use (80), (81), (83)–(85) and the results in Lemma 2 in Appendix B to simplify them.

$$\begin{aligned}T_1 &= \sigma^4\sum_{l_1=1}^{N}\sum_{l_3=1}^{N}\mathrm{tr}\{\mathbf{C}_{l_1,l_1,r}(\omega_a)\}\mathrm{tr}\{\mathbf{C}_{l_3,l_3,i}(\omega_b)\}\\ &= \sigma^4N^2\underbrace{\mathrm{tr}\{\mathbf{P}_r(\omega_a)\}}_{=0}\underbrace{\mathrm{tr}\{\mathbf{P}_i(\omega_b)\}}_{=0} = 0,\end{aligned} \tag{93}$$

$$\begin{aligned}T_2 &= \sigma^4\sum_{l_1=1}^{N}\sum_{l_2=1}^{N}\mathrm{tr}\{\mathbf{C}_{l_1,l_2,r}^T(\omega_a)\mathbf{C}_{l_1,l_2,i}(\omega_b)\}\\ &= \sigma^4\underbrace{\Big[\sum_{l_1=1}^{N}\varphi^{-(a+b)l_1}\Big]}_{=0}\underbrace{\Big[\sum_{l_2=1}^{N}\varphi^{(a+b)l_2}\Big]}_{=0}\mathrm{tr}\{\mathbf{P}_r^T(\omega_a)\mathbf{P}_i(\omega_b)\} = 0,\end{aligned} \tag{94}$$

$$
\begin{aligned}
T_3 &= \sigma^4 \sum_{l_1=1}^{N} \sum_{l_2=1}^{N} \mathrm{tr}\big\{\mathbf{C}_{l_1,l_2,r}(\omega_a)\mathbf{C}_{l_2,l_1,i}(\omega_b)\big\} \\
&= \sigma^4 \underbrace{\Big[\sum_{l_1=1}^{N} \varphi^{(b-a)l_1}\Big]}_{=\begin{cases}0 & a\neq b\\ N & a=b\end{cases}} \underbrace{\Big[\sum_{l_2=1}^{N} \varphi^{(a-b)l_2}\Big]}_{=\begin{cases}0 & a\neq b\\ N & a=b\end{cases}} \mathrm{tr}\big\{\mathbf{P}_r(\omega_a)\mathbf{P}_i(\omega_b)\big\} \\
&= \begin{cases} 0 & a \neq b \\ \sigma^4 N^2 \underbrace{\mathrm{tr}\big\{\mathbf{P}_r(\omega_a)\mathbf{P}_i(\omega_a)\big\}}_{=0} = 0 & a = b \end{cases}, \qquad (95)
\end{aligned}
$$

$$
\begin{aligned}
T_4 &= \sigma^2 \sum_{l_1=1}^{N} \sum_{l_2=1}^{N} \sum_{l_4=1}^{N} \boldsymbol{\epsilon}_{l_1}^T \mathbf{C}_{l_1,l_2,r}(\omega_a)\mathbf{C}_{l_2,l_4,i}(\omega_b)\boldsymbol{\epsilon}_{l_4} \\
&= \sigma^2 \underbrace{\Big[\sum_{l_1=1}^{N} \varphi^{a(1-l_1)}\boldsymbol{\epsilon}_{l_1}^T\Big]}_{=\hat{\boldsymbol{\epsilon}}^*(\omega_a)} \mathbf{P}_r(\omega_a) \underbrace{\Big[\sum_{l_2=1}^{N} \varphi^{(a-b)l_2}\Big]}_{=\begin{cases}0 & a\neq b\\ N & a=b\end{cases}} \mathbf{P}_i(\omega_b) \underbrace{\Big[\sum_{l_4=1}^{N} \varphi^{b(l_4-1)}\boldsymbol{\epsilon}_{l_4}\Big]}_{=\hat{\boldsymbol{\epsilon}}(\omega_b)} \varphi^{b-a} \\
&= \begin{cases} 0 & a \neq b \\ \sigma^2 N \hat{\boldsymbol{\epsilon}}^*(\omega_a)\mathbf{P}_r(\omega_a)\mathbf{P}_i(\omega_a)\hat{\boldsymbol{\epsilon}}(\omega_a) & a = b \end{cases}, \qquad (96)
\end{aligned}
$$

$$
\begin{aligned}
T_5 &= \sigma^2 \sum_{l_1=1}^{N} \sum_{l_2=1}^{N} \sum_{l_4=1}^{N} \boldsymbol{\epsilon}_{l_2}^T \mathbf{C}_{l_1,l_2,r}^T(\omega_a)\mathbf{C}_{l_1,l_4,i}(\omega_b)\boldsymbol{\epsilon}_{l_4} \\
&= \sigma^2 \underbrace{\Big[\sum_{l_1=1}^{N} \varphi^{-(a+b)l_1}\Big]}_{=0} \Big[\sum_{l_2=1}^{N} \varphi^{al_2}\boldsymbol{\epsilon}_{l_2}^T\Big] \mathbf{P}_r^T(\omega_a)\mathbf{P}_i(\omega_b) \Big[\sum_{l_4=1}^{N} \varphi^{bl_4}\boldsymbol{\epsilon}_{l_4}\Big] = 0, \qquad (97)
\end{aligned}
$$

$$
\begin{aligned}
T_6 &= \sigma^2 \sum_{l_1=1}^{N} \sum_{l_2=1}^{N} \sum_{l_3=1}^{N} \boldsymbol{\epsilon}_{l_3}^T \mathbf{C}_{l_3,l_2,i}(\omega_b)\mathbf{C}_{l_1,l_2,r}^T(\omega_a)\boldsymbol{\epsilon}_{l_1} \\
&= \sigma^2 \underbrace{\Big[\sum_{l_2=1}^{N} \varphi^{(a+b)l_2}\Big]}_{=0} \Big[\sum_{l_3=1}^{N} \varphi^{-bl_3}\boldsymbol{\epsilon}_{l_3}^T\Big] \mathbf{P}_i(\omega_b)\mathbf{P}_r^T(\omega_a) \Big[\sum_{l_1=1}^{N} \varphi^{-al_1}\boldsymbol{\epsilon}_{l_1}\Big] = 0, \qquad (98)
\end{aligned}
$$

$$T_7 = \sigma^2 \sum_{l_1=1}^{N} \sum_{l_2=1}^{N} \sum_{l_4=1}^{N} \boldsymbol{\epsilon}_{l_3}^T \mathbf{C}_{l_3,l_1,i}(\omega_b) \mathbf{C}_{l_1,l_2,r}(\omega_a) \boldsymbol{\epsilon}_{l_2}$$

$$= \sigma^2 \underbrace{\left[\sum_{l_3=1}^{N} \varphi^{b(1-l_3)} \boldsymbol{\epsilon}_{l_3}^T\right]}_{=\hat{\boldsymbol{\epsilon}}^*(\omega_b)} \mathbf{P}_i(\omega_b) \underbrace{\left[\sum_{l_1=1}^{N} \varphi^{(b-a)l_1}\right]}_{=\begin{cases} 0 & a \neq b \\ N & a = b \end{cases}} \mathbf{P}_r(\omega_a) \underbrace{\left[\sum_{l_2=1}^{N} \varphi^{a(l_2-1)} \boldsymbol{\epsilon}_{l_2}\right]}_{=\hat{\boldsymbol{\epsilon}}(\omega_a)} \varphi^{a-b}$$

$$= \begin{cases} 0 & a \neq b \\ \sigma^2 N \hat{\boldsymbol{\epsilon}}^*(\omega_a) \mathbf{P}_i(\omega_a) \mathbf{P}_r(\omega_a) \hat{\boldsymbol{\epsilon}}(\omega_a) & a = b \end{cases}. \tag{99}$$

All seven terms are zero for the case $a \neq b$. Two of the terms, T_4 and T_7, give a nonzero contribution for the case $a = b$. However, addition of these two terms gives

$$T_4 + T_7 = \sigma^2 N \hat{\boldsymbol{\epsilon}}^*(\omega_a) \underbrace{\big(\mathbf{P}_r(\omega_a)\mathbf{P}_i(\omega_a) + \mathbf{P}_i(\omega_a)\mathbf{P}_r(\omega_a)\big)}_{=0} \hat{\boldsymbol{\epsilon}}(\omega_a) \tag{100}$$

according to (72) in Lemma 2. We therefore get

$$\mathbf{G}_{12}(\omega_a, \omega_b) = 0, \qquad \forall\, a, b. \tag{101}$$

From (77)–(79) it is seen that the element

$$\mathbf{G}_{11}(\omega_a, \omega_b) = \mathrm{E}\left\{ \frac{\partial V\big(\mathbf{g}_\infty(\omega_a)\big)}{\partial \gamma_r} \cdot \frac{\partial V\big(\mathbf{g}_\infty(\omega_b)\big)}{\partial \gamma_r} \right\} \tag{102}$$

is given by the sum of the seven terms T_1–T_7 with $\mathbf{P}_i(\omega_k)$ replaced by $\mathbf{P}_r(\omega_k)$. The new terms, which we denote S_1–S_7, have the values

$$S_1 = 0, \tag{103}$$
$$S_2 = 0, \tag{104}$$

$$S_3 = \begin{cases} 0 & a \neq b \\ \sigma^4 N^2 \mathrm{tr}\{\mathbf{P}_r^2(\omega_a)\} & a = b \end{cases}, \tag{105}$$

$$S_4 = \begin{cases} 0 & a \neq b \\ \sigma^2 N \hat{\boldsymbol{\epsilon}}^*(\omega_a) \mathbf{P}_r^2(\omega_a) \hat{\boldsymbol{\epsilon}}(\omega_a) & a = b \end{cases}, \tag{106}$$

$$S_5 = 0, \tag{107}$$
$$S_6 = 0, \tag{108}$$

$$S_7 = \begin{cases} 0 & a \neq b \\ \sigma^2 N \hat{\boldsymbol{\epsilon}}^*(\omega_a) \mathbf{P}_r^2(\omega_a) \hat{\boldsymbol{\epsilon}}(\omega_a) & a = b \end{cases} \tag{109}$$

and hence

$$\mathbf{G}_{11}(\omega_a, \omega_b) = \begin{cases} 0 & a \neq b \\ \sigma^4 N^2 \mathrm{tr}\{\mathbf{P}_r^2(\omega_a)\} + 2\sigma^2 N \hat{\boldsymbol{\epsilon}}^*(\omega_a) \mathbf{P}_r^2(\omega_a) \hat{\boldsymbol{\epsilon}}(\omega_a) & a = b \end{cases}. \tag{110}$$

Finally, the element $\mathbf{G}_{21}(\omega_a, \omega_b) = \mathbf{G}_{12}(\omega_a, \omega_b)$, and the element $\mathbf{G}_{22}(\omega_a, \omega_b)$ is obtained by changing $\mathbf{P}_r(\omega_k)$ to $\mathbf{P}_i(\omega_k)$ in (110).

D The standard linear solid model

The standard linear solid model [12] in Figure 11 is a commonly used parametric model for the complex modulus. The model has two springs and one dashpot and is useful for low to moderately high frequencies. We will derive the complex modulus $E(\omega, \boldsymbol{\theta})$ given by the model, where the model parameter is

$$\boldsymbol{\theta} = (E_1, E_2, \eta)^T. \tag{111}$$

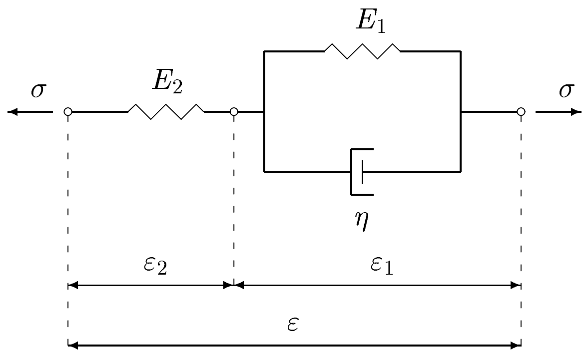

Figure 11: The standard linear solid model.

The compatibility (geometrical) relation

$$\varepsilon = \varepsilon_1 + \varepsilon_2 \tag{112}$$

and the constitutive relation

$$\sigma = E_1\varepsilon_1 + \eta\dot{\varepsilon}_1 = E_2\varepsilon_2, \tag{113}$$

where σ denotes stress and ε denotes strain, can be obtained from Figure 11. Elimination of ε_1 and ε_2 in (112) and (113) gives

$$\sigma = E_1(\varepsilon - \frac{\sigma}{E_2}) + \eta(\dot{\varepsilon} - \frac{\dot{\sigma}}{E_2}) \tag{114}$$

and after Fourier transformation

$$\hat{\sigma} = E_1(\hat{\varepsilon} - \frac{\hat{\sigma}}{E_2}) + \eta(\mathrm{i}\omega\hat{\varepsilon} - \frac{\mathrm{i}\omega\hat{\sigma}}{E_2}). \tag{115}$$

Finally, the complex modulus given by the model is

$$E(\omega, \boldsymbol{\theta}) = \frac{\hat{\sigma}}{\hat{\varepsilon}} = \frac{E_2(E_1 + \mathrm{i}\omega\eta)}{E_1 + E_2 + \mathrm{i}\omega\eta}, \tag{116}$$

where $\hat{\sigma}/\hat{\varepsilon}$ is established from (115).